New developments in simulating X-ray phase contrast imaging

A. Peterzol [1,*], J. Berthier [1], P. Duvauchelle [1], C. Ferrero [2], and D. Babot [1]

[1]Institut National des Sciences Appliquées de Lyon, Laboratoire de Contrôle Non Destructif par Rayonnements Ionisants (CNDRI), 20 Av. A. Einstein, 69621 Villeurbanne, France

[2]European Synchrotron Radiation Facility, BP220 rue Horowitz, 38043 Grenoble, France

Abstract

A deterministic algorithm simulating phase contrast (PC) x-ray images for complex 3-dimensional (3D) objects is presented. This algorithm has been implemented in a simulation code named VXI (Virtual X-ray Imaging). The physical model chosen to account for PC technique is based on the Fresnel-Kirchhoff diffraction theory.
The algorithm consists mainly of two parts. The first one exploits the VXI ray-tracing approach to compute the object transmission function. The second part simulates the PC image due to the wave front distortion introduced by the sample.
In the first part, the use of computer-aided drawing (CAD) models enables simulations to be carried out with complex 3D objects. Differently from the VXI original version, which makes use of an object description via triangular facets, the new code requires a more "sophisticated" object representation based on Non-Uniform Rational B-Splines (NURBS).
As a first step we produce a spatial high resolution image by using a point and monochromatic source and an ideal detector. To simulate the polychromatic case, the intensity image is integrated over the considered x-ray energy spectrum. Then, in order to account for the system spatial resolution properties, the high spatial resolution image (mono or polychromatic) is convolved with the total point spread function of the imaging system under consideration.
The results supplied by the presented algorithm are examined with the help of some relevant examples.

PACS: 81.70.-q, 87.59.Bh, 42.15.Dp, 42.50.Dr

Keywords: Phase contrast, X-ray imaging, Deterministic Simulation, Ray-tracing

1. Introduction

Phase contrast x-ray imaging [1-11] has been for almost 10 years a very active field of x-ray science since the technique offers greatly enhanced image quality over conventional radiology . Phase contrast (PC) arises because both the amplitude and phase of x-rays are

* corresponding author.
email address: angela.peterzol@insa-lyon.fr

modified as an x-ray beam propagates through an object. A detailed understanding of the underlying physics requires that the radiation be treated as a wave field rather than by means of simple geometrical optics. In that context, a big effort has been dedicated to develop a comprehensive theory for PC imaging [4,6,9-11].
Moreover, to develop and optimize a new imaging system, and to recognize the influence of the various adjustable parameters, simulation can be a helpful tool for the development of clinical and industrial applications of this promising technique.
In previous papers [12-14], it was reported on a computer code developed to simulate the operation of radiographic, radioscopic or tomographic systems. This code, named VXI (virtual x-ray imaging), is based on ray tracing techniques and is completely deterministic. It enables to simulate direct images [12] and first-order scattering [13,14] in complex configurations (intricate three-dimensional (3D) objects, polychromatic spectra, focal spots causing geometric unsharpness,…).
Here, we present the implementation of an algorithm designed to simulate x-ray PC images of complex 3D objects in the VXI code [15]. The results obtained by this code are examined with the help of some representative examples.

2. Theory of phase contrast imaging

Most of the theoretical frameworks found in the literature, [1-4,6,11] being some examples, and describing the so-called in-line PC imaging are based on the Fresnel-Kirchhoff diffraction theory [16]. In the following the latter is briefly reviewed and the fundamental equations which VXI PC is based on are recalled. More details can be found in [11], where the general principles of the in-line PC imaging for spatially incoherent sources, such as x-ray tubes, are investigated.
In order to apply the Kirchhoff's integral [16] to PC imaging, let us first consider a monochromatic spherical wave of wavelength λ, generated from a point source located at the point P_0 of coordinates $(x_0,y_0,-r_0)$ (see Fig. 1), and propagating through a sample virtually lying on the so-called object plane, which is positioned just after the sample and perpendicular to the z axis. The distance source-to-object plane is r_0. In order to write the diffracted wave field in $P(x_1,y_1,r_1)$ at a distance r_1 from the object plane, we assume that the wave field at the object plane $U(x,y,z=0)$ can be expressed as the product of an object transmission function $t(x,y)$ with $U_0(x,y,z=0)$, i.e. the spherical wave that would have been observed at the object plane in the absence of the sample.
We assume also that there exists a finite surface A on the object plane outside which $t(x,y)=1$. Under these circumstances, the wave perturbation in P can be written as

$$U(x_1, y_1, r_1) = U_0(x_1, y_1, r_1)(1 + c(x_1, y_1, r_1)) \quad (1)$$

where $U_0(x_1,y_1,r_1)$ represents the spherical wave that would have been detected at the image plane to which P belongs, in the absence of the sample (free space propagation), and the term $c(x_1,y_1,r_1)$ is the function related to the formation of the PC image. In the small angle or paraxial approximation [16], $c(x_1,y_1,r_1)$ is given by

$$c(x_1,y_1)=\frac{M}{i\lambda r_1}e^{-i\frac{\pi}{\lambda}\left[\frac{(x_1-x_0)^2+(y_1-y_0)^2}{(r_0+r_1)}\right]}\int_{-\infty}^{+\infty}\int_{-\infty}^{+\infty}dxdy\left(t(x,y)-1\right)e^{i\frac{\pi}{\lambda}\left[\frac{(x-x_0)^2+(y-y_0)^2}{r_0}+\frac{(x-x_1)^2+(y-y_1)^2}{r_1}\right]} \tag{2}$$

where, for the sake of simplicity, the *z* coordinate has been omitted, $M=(r_0+r_1)/r_0$ represents the image magnification, and *s* denotes the distance between P_0 and the image plane point (x_1,y_1), while s_0 and s_1 denote the distances from P_0 and P to the object plane point $(x,y,z=0)$, respectively.
From equation (1) it is straightforward to write the normalized intensity $in(x_1,y_1)$ as

$$in(x_1,y_1)=\left|1+c(x_1,y_1)\right|^2 \tag{3}$$

where we chose to normalize the intensity I to I_0, i.e. the x-ray beam intensity that would have been detected on the image plane at the P position in the absence of the sample ($I=|U|^2$ *and* $I_0=|U_0|^2$).
In order to simulate the beam intensity at the P position, the convolution integral in equation (2) has to be computed numerically. This procedure can be facilitated if working in Fourier space [17].
The transmission function $t(x,y)$ represents the phase shift and the attenuation effect due to the sample. In literature, [4-6] being same examples, $t(x,y)$ is usually written as

$$t(x,y)=\exp\left(i\phi(x,y)-B(x,y)\right) \tag{4}$$

where $\Phi(x,y)$ and $B(x,y)$ correspond to the object phase and linear attenuation term, respectively. The definitions of $\Phi(x,y)$ and $B(x,y)$ are:

$$\phi(x,y)=\frac{-2\pi}{\lambda}\int dr\,\delta(x,y,z)$$
$$B(x,y)=\frac{2\pi}{\lambda}\int dr\,\beta(x,y,z) \tag{5}$$

where the integration is performed along the direction linking the source point P_0 and the object plane position (x,y). $\delta(x,y,z)$ and $\beta(x,y,z)$ are the 3D distributions of the real and imaginary part, respectively, of the x-ray refractive index *n* decrement

$$n=1-\delta+i\beta \tag{6}$$

$\Phi(x,y)$ and $B(x,y)$ represent the projections of the object's $\delta(x,y,z)$ and $\beta(x,y,z)$, respectively, along the x-ray travelling direction. In order to be able to model an object via (4) and (5), the object is supposed to be "thin" for x-rays so that the projection approximation holds true. If d is the object thickness, the object can be deemed thin [5] as long as the size of the finest feature to image is larger than $(\lambda d)^{0.5}$.
It is important to underline that, to our knowledge, the formulas describing the x-ray

beam intensity impinging upon image planes reported in literature, -and as a consequence the corresponding signal simulations-, are based on two important assumptions: (i) small angle approximation, which justifies the use of (2) and (ii) the projection approximation, which allows to describe the object transmission function by (4) and (5).

Up to now the mathematical PC framework we presented assumes a monochromatic point source and an ideal detector. In practice, the source has a finite size and the image detector has a limit on the maximum detectable spatial frequency.
The intensity distribution in the image obtained with a totally incoherent, finite size source and a finite resolution detector is the convolution of the intensity distribution in the image corresponding to the point source and the system point spread function (PSF) [11]. The latter is the convolution of two functions, the geometric PSF, which represents the effect of the geometric blurring caused by the size and shape of the focal spot and the magnification factor used, and the PSF of the acquisition device.
Another aspect which has to be taken into account is the temporal coherence of the source. Differently from synchrotron x-ray facilities, which can provide monochromatic beams ($\Delta E/E \sim 10^{-4}$), x-ray tubes are actually polychromatic sources. In such a case it is necessary to integrate the intensity formula over the emitted spectrum [16].

3. The VXI PC code

As previously mentioned, VXI is a computer code developed to simulate the operation of radiographic, radioscopic or tomographic devices [12-14]. The completely deterministic simulation is based on ray-tracing techniques and on the x-ray attenuation law. In order to be able to carry out image simulations with a large variety of samples, the code was designed to accept CAD files in standard format to describe the sample geometry. Many software packages enable complex 3D objects to be drawn and CAD files to be generated, for example in stereolithographic (STL) format. These files contain a list of nodes and meshes (triangular facets) that approximate the object surface. The precision of the approximation, which is linked to the size of the meshes, can be adjusted. The object may consist of different parts, possibly made of different materials, assumed to be homogeneous. The CAD model of each part can be processed independently.
Once the object and the position of the point source are defined, a set of rays is emitted from the source towards every pixel centre of the detector (see Fig. 2). Each ray may intersect a certain number of meshes at the sample surface or at the interfaces between different parts of the object. The path length in every part of the object is calculated by determining the coordinates of all the intersection points.
This procedure, which is used in the VXI code to compute the number of photons $N(E)$ which emerge from the sample and reach a pixel of the detector (eq. (1) in [12]), can be applied to compute the $\delta(x,y,z)$ and $\beta(x,y,z)$ projections along the x-ray travelling direction, i.e. $\Phi(x,y)$ and $B(x,y)$. In this way it is possible to evaluate the 2D map of the transmission function $t(x,y)$ on the object plane. For this purpose a virtual detector plane is positioned just after the sample, and for every pixel coordinates (x_n,y_m) at the detector plane the total path length d_i through each material i of the object is calculated. Subsequently, $\Phi(x_n,y_m)$ and $B(x_n,y_m)$ are computed as

$$\phi(x_n, y_m, E) = \frac{-2\pi}{\lambda} \sum_i \delta_i(E) d_i$$

$$B(x_n, y_m, E) = \frac{2\pi}{\lambda} \sum_i \beta_i(E) d_i \qquad (7)$$

where $\delta_i(E)$ and $\beta_i(E)$ designate the real and imaginary part, respectively, of the refraction index decrement associated with the material i at the energy E.
Therefore, with a simple modification of the VXI code it is possible to compute the 2D map of the object transmission function $t(x,y)$. Given the latter, the PC signal can be simulated by computation of the parameter c exploiting a discrete fast Fourier transform algorithm, which reduces the computation time in comparison with the numerical integration.
Once the parameter c has been worked out, the relative intensity image is derived in accordance with equation (3). This is a spatial high resolution image, which assumes a monochromatic point source. In order to reproduce the case of a polychromatic x-ray source, the intensity image is computed as a weighted sum of all monoenergetic images obtained for each energy E_i belonging to the considered spectrum. The latter is treated as input information such as for example the source-to-object distance r_0.
The last step consists in convolving the spatial high resolution polychromatic image with the PSF of the imaging system being considered.

4. The effects of the CAD model on PC image simulation

With our method it is possible to simulate the PC signals of a wide range of 3D complex objects. By now, mainly the intensity patterns of edges [3], cylindrical phantoms [5,7,10], and spheres [2,8], for which the analytical calculation of phase and attenuation projections is straightforward, have been reported.
For this reason the software was firstly tested by simulating the PC images of cylinders and spheres. In particular, the 2D map of $t(x,y)$ was computed 1) analytically and 2) using VXI, and the corresponding image intensities were compared. By that it was possible to point out the "weak points" of the 3D-object CAD representation. As an example, the CAD facetted model of a sphere (radius=150 μm) is reported in Fig. 3.
While this object "discretisation" does not pose any problem (the object "sampling step" is supposed to be sufficiently smaller than the detector pixel size) in simple attenuation imaging, it introduces not negligible artefacts in the PC case, since $t(x,y)$ has to be known/sampled with a precision of one micrometer or even less [15].
In Figs. 4(a) and 4(b) are reported the intensity images at 1m sample-to-detector distance for a PMMA sample sphere of 150 μm radius irradiated with a parallel monochromatic beam of 15 keV, calculated using the analytical and the VXI transmission function, respectively. In both cases $t(x,y)$ was mapped with 0.2 μm precision. The VXI image presents the artefacts due to the facetted CAD model (Fig. 3). In fact, the facetted object contains a Fourier component due to the quasi–periodic object description: the frequency

of the triangular facets repetition comes up in the PC signal.
It has to be pointed out that in general the PC signal depends only on the derivative terms (of different orders) of the phase: for example, the intensity distribution in the image of a pure phase object is proportional (in the low spatial resolution approximation) to the Laplacian of the phase distribution in the object wave. Hence, the image reveals the object edges, which are typically associated with a dark-white fringe structure.
Differently from conventional radiography, the PC technique is very sensitive to derivative discontinuities of *t(x,y)*. Returning to Fig. 4, the artefacts introduced by the facetted model can persist even after the spatial resolution properties of the specific imaging system are taken into account. As an example, the intensity images of Figs. 4(a) and 4(b), are reported in Fig.s 4(c) and 4(d), respectively, after convolution with the PSF:

$$PSF(x,y) = \left(erf\left[a_x(x-b_x)\right] - erf\left[a_x(x-c_x)\right]\right)\left(erf\left[a_y(y-b_y)\right] - erf\left[a_y(y-c_y)\right]\right) \qquad (8)$$

where *erf* is the error function, and $a_{x,y}$, $b_{x,y}$ and $c_{x,y}$ are parameters defined as follows: the quantity ($c_{x,y}$-$b_{x,y}$) corresponds to the FWHMs along the *x*,*y* directions of the PSF, which have been set equal to 30 μm for both the *x*,*y* axes, since this value represents the smallest pixel size for digital mammography systems (SenoScan Digital Mammography system, Fischer Imaging Corporation, Denver, USA). In practice, (10) represents the 2D extension of equation (1) in [18]. The parameters $a_{x,y}$ indicate the spreading of the PSF along the *x*,*y* directions and were set equal to 0.2 μm^{-1} for both axes. This spreading is associated with the PSF used to produce the images of Figs. 4(c) and 4(d). Here, the high frequency signal contribution to $I/I_{0,}$ which was present in the data prior to convolution, has been removed and the image contrast has been significantly reduced. Nevertheless, Fig. 4(d) still presents the faceting artefacts even if the difference between the two images (generated with the two different *t(x,y)*) is smaller than the original unconvolved case. In Fig. 4(e), which shows the intensity profiles (passing through the sphere centre) extracted from Figs. 4(c) and 4(d), one can clearly see the low frequency oscillations inside the sphere originating from the CAD model.
From these preliminary examples, it clearly emerges that a PC simulation tool needs an exact object modelling. For this reason a new CAD object description has been envisaged and the related code has been developed. The 3D objects are described following a parametric approach.
In particular, the present CAD model makes use of Non-Uniform Rational B-Splines (NURBS) [19], which offer one common mathematical basis to represent both standard analytical shapes (e.g. conic sections and quadric surfaces) and free form shapes while maintaining mathematical exactness and resolution independence.
As a first example of object representation by NURBS in VXI, the intensity image of the usual PMMA sphere is illustrated in Fig. 4(f). In this case all the artefacts present in Fig. 4(b) vanished. In addition, there is an excellent agreement (differences less than 5%) between the images obtained analytically and those computed using the NURBS model.
The CAD NURBS model was therefore adopted as a basis for the new VXI version, by means of which it is possible to compute the PC images of all 3D complex objects describable in the IGES or STEP file format, which are standard formats making provision for the NURBS geometric entity description in CAD tools.
As another example, let us consider the four 3D objects of different shapes contained in a

bounding box of 1.5 mm side (see Fig. 5). The objects are supposed to be made of PMMA and irradiated with a polychromatic x-ray beam impinging on the box side indicated by the arrow in Fig. 5; the *t(x,y)* sampling step is 0.5 μm and r_1=1 m. The x-ray spectrum is a typical mammography spectrum obtainable at 30 kV with a Molybdenum (Mo) anode target and with a 0.03 mm Mo filter. This spectrum presents two characteristic lines at 17.4 and 19.6 keV, and allows reducing the PC signal degradation due to the deployment of a polychromatic beam as compared to a broader spectrum without lines. Actually, the PC image in Fig. 6(a), which corresponds to the four objects in Fig. 5 displays a good contrast (the peak-to-peak difference at the object edges is about 1.8 in a relative intensity scale).
For comparison purposes the image with the objects of Fig. 5 obtained using the facetted model for the evaluation of *t(x,y)* is also shown in Fig. 6(b). In this case, the image exhibits the low frequency periodic artefacts.
Also in this case, the high spatial resolution (0.5 μm) images have been convolved with the PSF defined in (10). The convolution effects are clearly noticeable in Figs. 6(c) and 6(d) (compare with Figs. 6(a) and 6(b)).
After convolution, the difference between the images obtained using the two different CAD models becomes smaller, since the convolution reduces the artefacts without eliminating them completely.

5. Conclusions and future perspectives

A computer code able to simulate PC images has been presented. The code is based on the Fresnel-Kirchhoff diffraction theory and computes the object transmission function *t(x,y)* according to the classical projection approximation.
The code is designed to process CAD object files containing a facetted sample description and also objects described by NURBS. This second approach has been followed, after observing that the polyhedral object representation introduces not negligible artefacts in the PC images, since the PC technique is very sensitive to discontinuities of the *t(x,y)* derivatives.
The advantage of the NURBS description of surfaces is that of providing geometrically smooth objects, thus not causing artefacts. The results supplied by the NURBS code version are of doubtlessly better quality.
However, the facetted sample description can be steel useful for describing biological samples for which it is not possible to use CAD tools [12]. In these cases, the artefacts involved by the polyhedral description are less detectable when considering a low spatial resolution system as it is the case of conventional medical imaging.
PC VXI is a useful tool for estimating the achievable image quality of complex 3D objects in the PC imaging technique. It takes into account the properties of the source (size, energy spectrum) and the detector (PSF).
It can be employed at synchrotron or lab facilities dealing with PC experiments or [20-23] developing systems for PC imaging.
Prospectively we envisage to improve the model for the transmission function *t(x,y)*. The new *t(x,y)* evaluation will take into account the refraction of x-rays as they pass through the sample. The aim of this approach is to provide a simulation tool capable to account for PC imaging of thick samples (several cm) under spatial high resolution conditions (1

μm or less).

Acknowledgments

The authors gratefully acknowledge A. Bravin for the many constructive discussions they had with him. P. Bleuet, M. Sanchez del Rio are also acknowledged for their useful suggestions and enthusiastic participation in the initial phase of the present investigation. The authors thank the French Ministry of National Education, Advanced Education, and Research for supporting this work and are very grateful to the IN2P3's Computing Centre for providing them with computing resources and assistance.

References

1. G. Margaritondo and G. Tromba, 'Coherence-based edge diffraction sharpening of x-ray images: A simple model,' J. Appl. Phys. 85 (1999) 3406-3408
2. T. E. Gureyev, C. Raven, A. Snigirev, I. Snigireva, and S. W. Wilkins, 'Hard x-ray quantitative non-interferometric phase-contrast microscopy,' J. Phys. D: Appl. Phys. 32 (1999) 563-567
3. Y. Hwu, Wen-Li Tsai, A. Groso, G. Margaritondo, and Jung Ho Je, 'Coherence-enhanced synchrotron radiology: Simple theory and practical applications,' J. Phys. D: Appl. Phys. 35 (2002) R105-R120
4. X. Wu and H. Liu, 'A general theoretical formalism for X-ray phase contrast imaging,' J. X-Ray Sci. Technol. 11 (2003) 33-42
5. X. Wu and H. Liu, 'Clinical implementation of x-ray phase-contrast imaging: Theoretical Foundations and design considerations,' Med. Phys. 30 (2003) 2169-2179
6. K. M. Pavlov, T. E. Gureyev, D. Paganin, Ya I. Nesterets, M. J. Morgan, and S. W. Wilkins, 'Linear systems with slowly varying transfer functions and their application to x-ray phase-contrast imaging,' J. Phys. D: Appl. Phys. 37 (2004) 2746-2750
7. P. Monnin and S. Bulling, 'Quantitative characterization of edge enhancement in phase contrast x-ray imaging,' Med. Phys. 31 (2004) 1372-1383
8. M. J. Kitchen, D. Paganin, R. A. Lewis, N. Yagi, K. Uesegi, and S. T. Mudie, 'On the origin of speckle in x-ray phase contrast images of lung tissue,' Phys. Med. Biol. 49 (2004) 4335-4348
9. X. Liu and H. Liu, 'A new theory of phase-contrast x-ray imaging based on Wigner distributions,' Med. Phys. 31 (2004) 2378-2384
10. A. Peterzol, A. Olivo, L. Rigon, S. Pani, and D. Dreossi, 'The effects of the imaging system on the validity limits of the ray-optical approach to phase contrast imaging', Medical Physics 32 (2005) 3617-3627
11. Ya I. Nesterets, S. W. Wilkins, T. E. Gureyev, A. Pogany, and A. W. Stevenson, 'On the optimization of experimental parameters for x-ray in-line phase-contrast imaging', Rev. Sci. Instr. 76, Art. No. 093707 (2005)

12. P. Duvauchelle, N. Freud, V. Kaftandjian, and D. Babot, 'A computer code to simulate X-ray imaging techniques,' NIM B 170 (2000) 245-258
13. N. Freud, P. Duvauchelle, and D. Babot, 'New developments in virtual x-ray imaging: fast simulation using a deterministic approach,' AIP Conf. Proc. 657 (2003) 553
14. N. Freud, P. Duvauchelle, S. A. Pistrui-Maximean, J. M. Létang, and D. Babot, 'Deterministic simulation of first-order scattering in virtual X-ray imaging,' NIM B 222 (2004) 285-300
15. A. Peterzol, J. Berthier, P. Duvauchelle, C. Ferrero, and D.Babot, 'X-ray phase contrast image simulation,' NIM B 254 (2007) 307-318
16. M. Born and E. Wolf, *Principles of Optics* (Pergamon, Oxford, 1975)
17. R. N. Bracewell, *The Fourier Transform and its Applications* (second ed., McGraw-Collina, New York NY 1986)
18. A. Peterzol, A. Bravin, P. Coan, and H. Elleaume, 'Image quality evaluation of the angiography imaging system at the European synchrotron radiation facility,' Nucl. Instrum. Methods A 510 (2003) 45-50
19. Les Piegl & Wayne Tiller: *The NURBS Book*, Springer-Verlag 1995-1997 (2nd ed)
20. E. F. Donnelly and R. R. Price, 'Quantification of the effect of kVp on edge-enhancement index in phase-contrast radiography,' Med. Phys. 29 (2002) 999-1002
21. A. Krol, A. Ikhlef, J. C. Kieffer, D. A. Bassano, C. C. Chamberlain, Z. Jiang, H. Pépin, and S. C. Prasad, 'Laser-based microfocused x-ray source for mammography: Feasibility study,' Med. Phys. 24 (1997) 725-732
22. C. Gaudin, M. Lamoureux, and C. Rouillé, 'X-ray emission from a compact hot plasma: applications to radiology and mammography,' Phys. Med. Biol. 46 (2001) 835-851
23. C. Honda, H. Ohara, A. Ishisaka, F. Shimada, and T. Endo, 'X-ray phase imaging using a X-ray tube with a small focal spot -improvement of image quality in mammography-,' Igaku Butsuri 22 (2002) 21-29

Figure captions

Fig. 1. Schematic display of the wave-optical approach to the PC formation mechanism for a circular cross-section object being irradiated by a spherical and monochromatic x-ray wave generated by a point source located at a distance r_0 from the object plane. The image is detected at a distance r_1 from the latter.

Fig. 2. Principle of the VXI simulation code. The ray SK intersects two meshes in the points A and B. Geometrical calculations enable determining the attenuation path length AB. Ray (1): transmitted photons. Rays (2) and (3): scattered photons.

Fig. 3. The CAD facetted model of a 150 μm radius PMMA sphere.

Fig. 4. Simulated images for a 150 μm radius PMMA sphere, assuming a parallel and

monochromatic beam of 15 keV and an ideal detector. They were computed using the analytical (a), the facetted CAD (b), and the new NURBS CAD (f) approach to the transmission function evaluation. The images (c) and (d) are the results of the convolution of the images (a) and (b), respectively, with the 30 μm FWHM detector response function (equation (8). The central profiles extracted from the sphere images (c) and (d) are reported in (e).

Fig. 5. 3D objects of different shapes "virtually" contained in a cube of 1.5 mm side. For the purposes of the simulation, the objects were supposed to be PMMA made and irradiated with a polychromatic x-ray beam impinging on the side indicated by the arrow.

Fig. 6. Simulated images corresponding to the four objects of Fig. 5, as obtained with the polychromatic beam for mammography applications and an ideal detector. The images were obtained using the NURBS CAD (a), and the facetted CAD (b) models, respectively for the transmission function evaluation. The images (c) and (d) are the results of the convolution of the images (a) and (b), respectively, with the detector PSF (equation (8)).

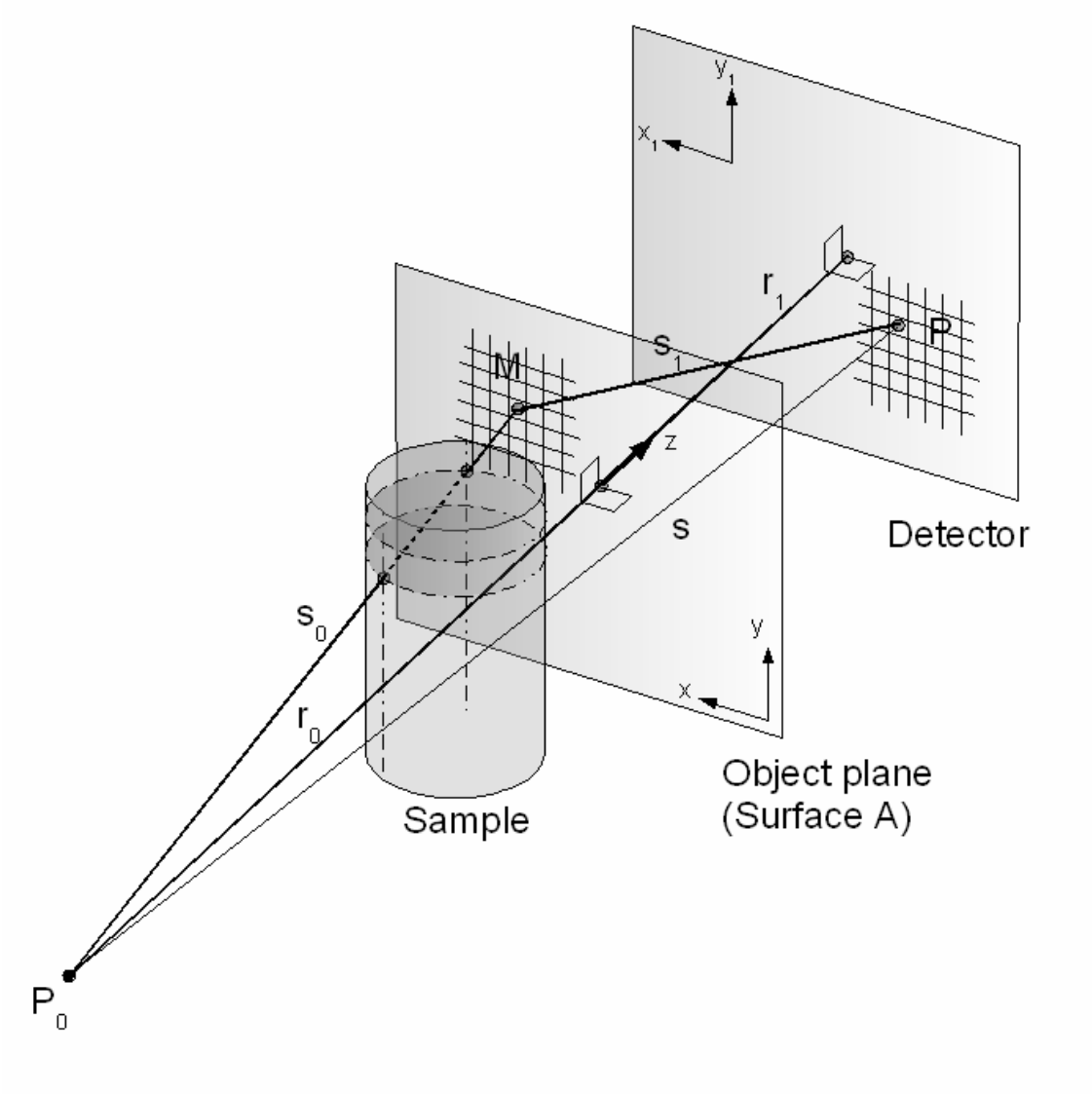
y1
x1
r1
s1
P
M
z
s
Detector
s0
r0
y
x
Object plane
(Surface A)
Sample
P0

Fig. 1

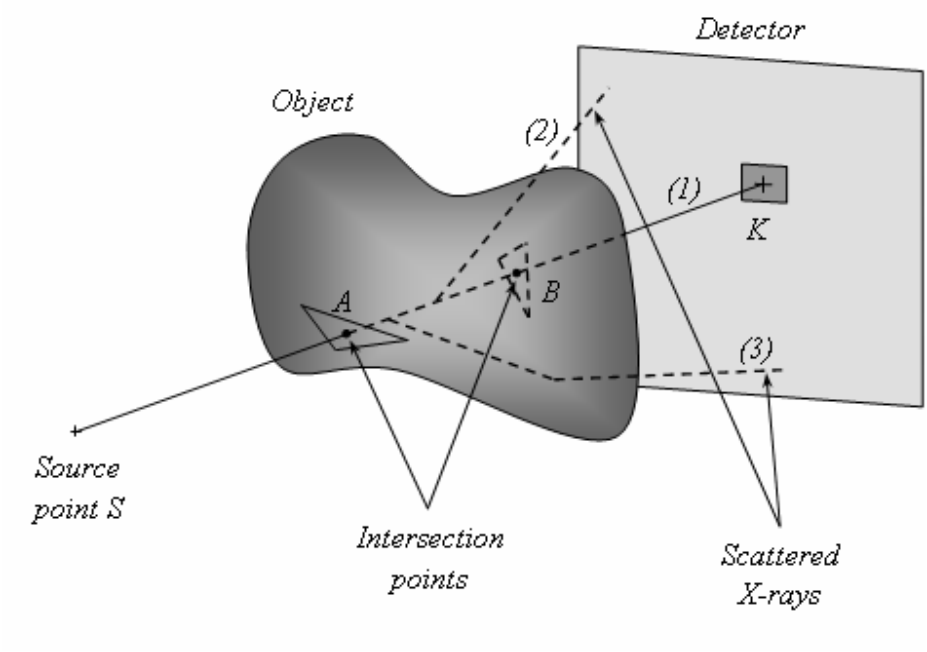
Detector
Object
(2)
(1)
K
A
B
(3)
Source
point S
Intersection
points
Scattered
X-rays

Fig. 2

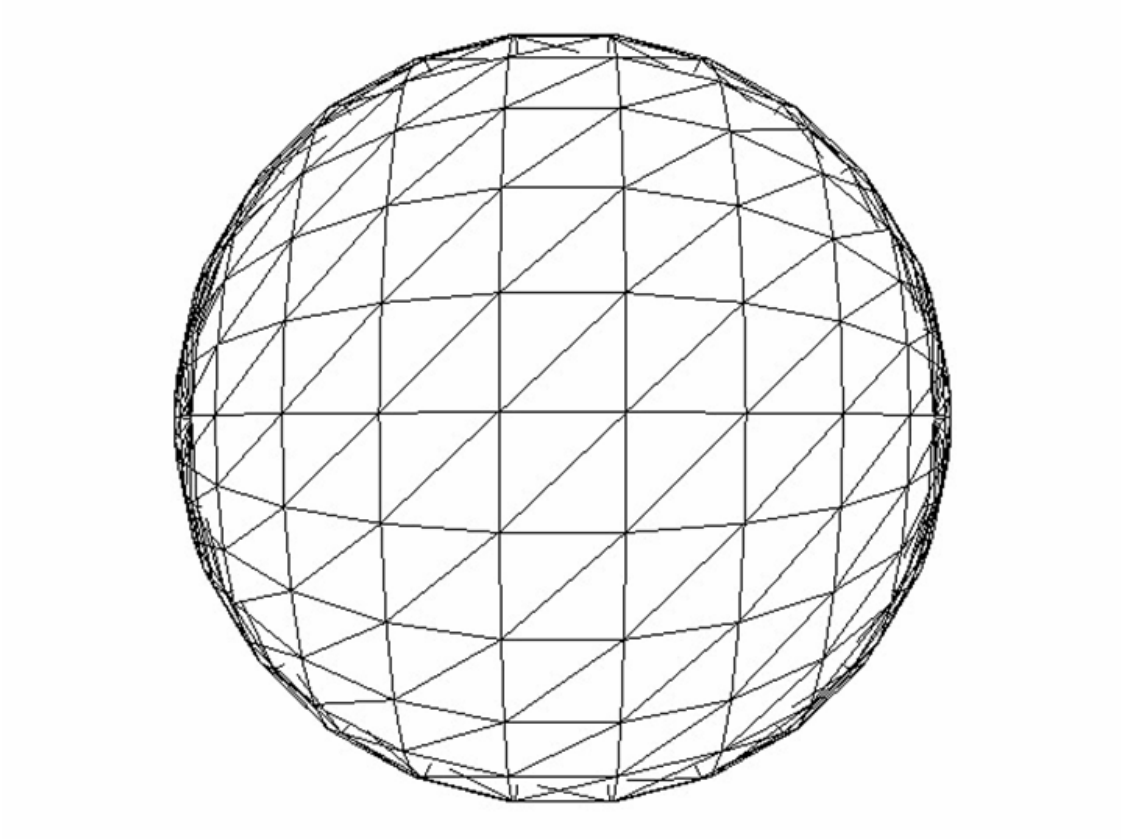

Fig. 3

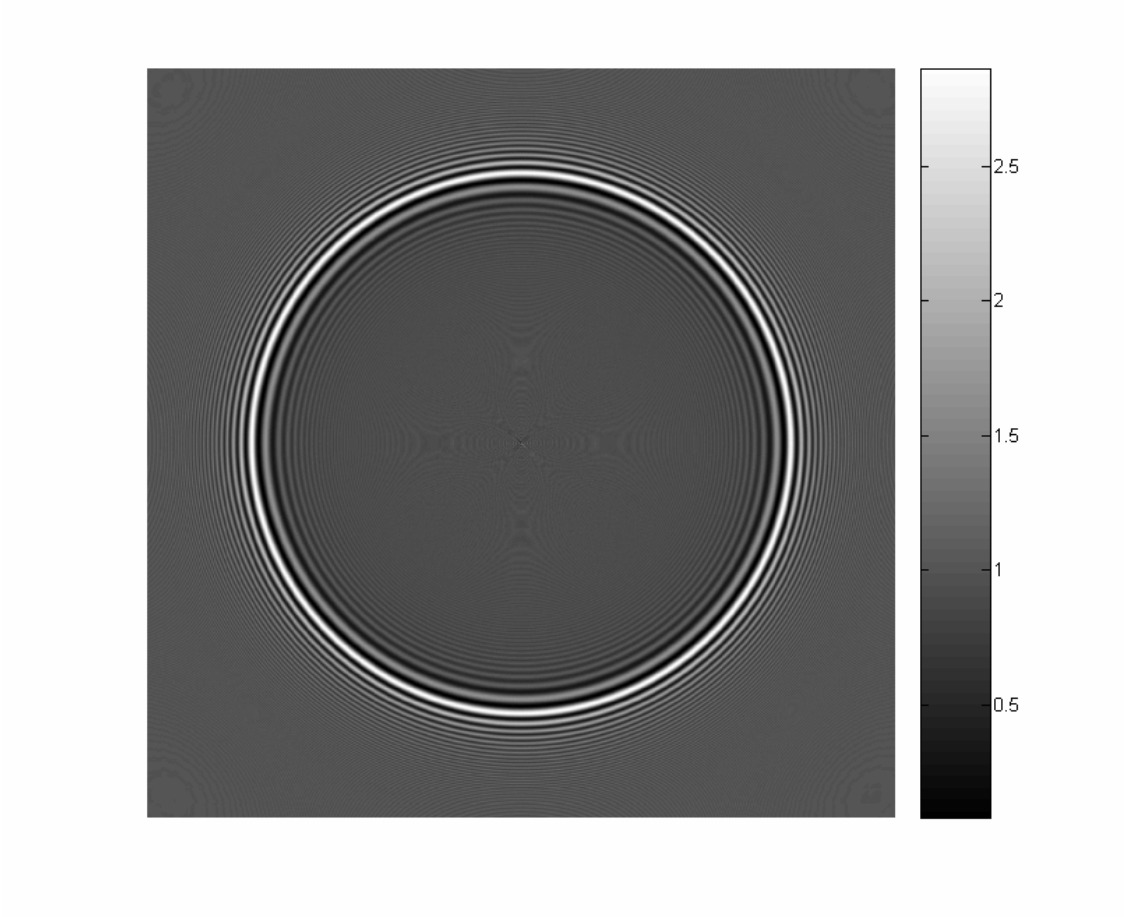

Fig. 4a

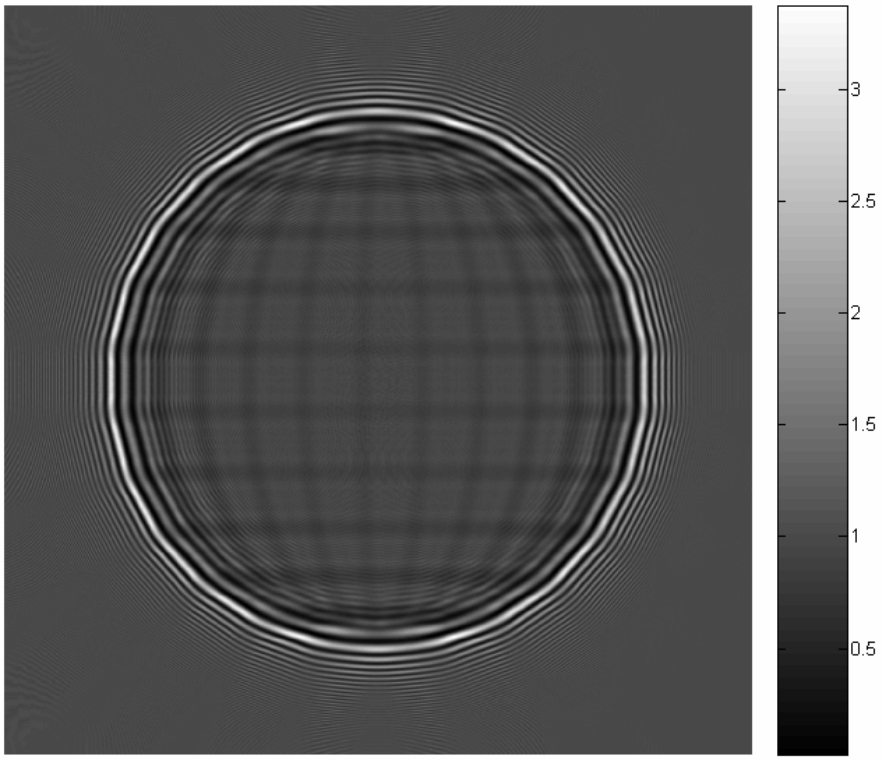

Fig. 4b

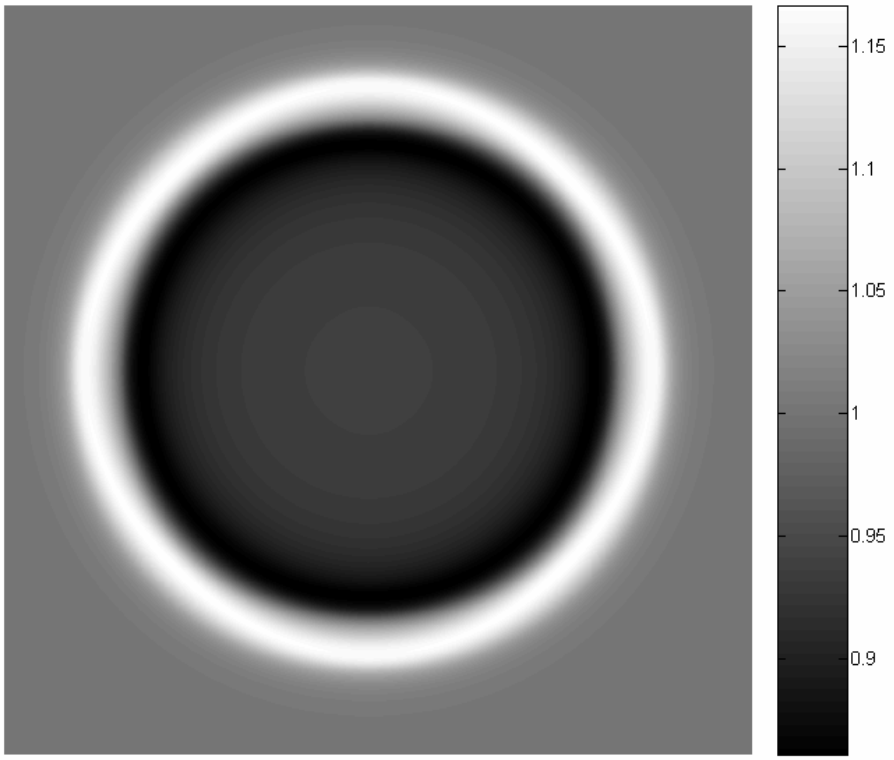

Fig. 4c

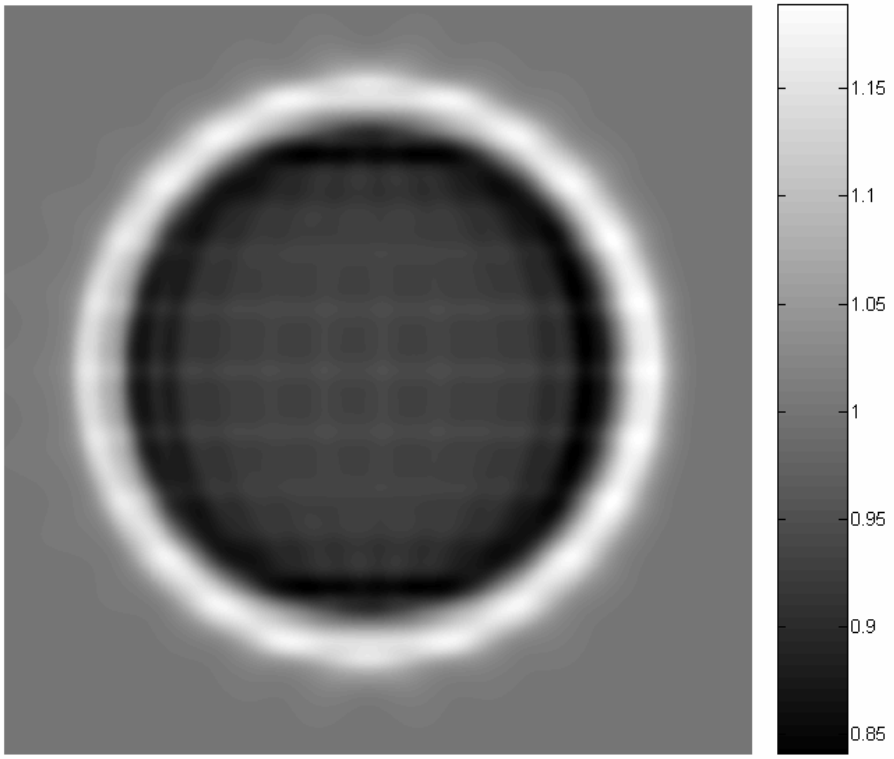

Fig. 4d

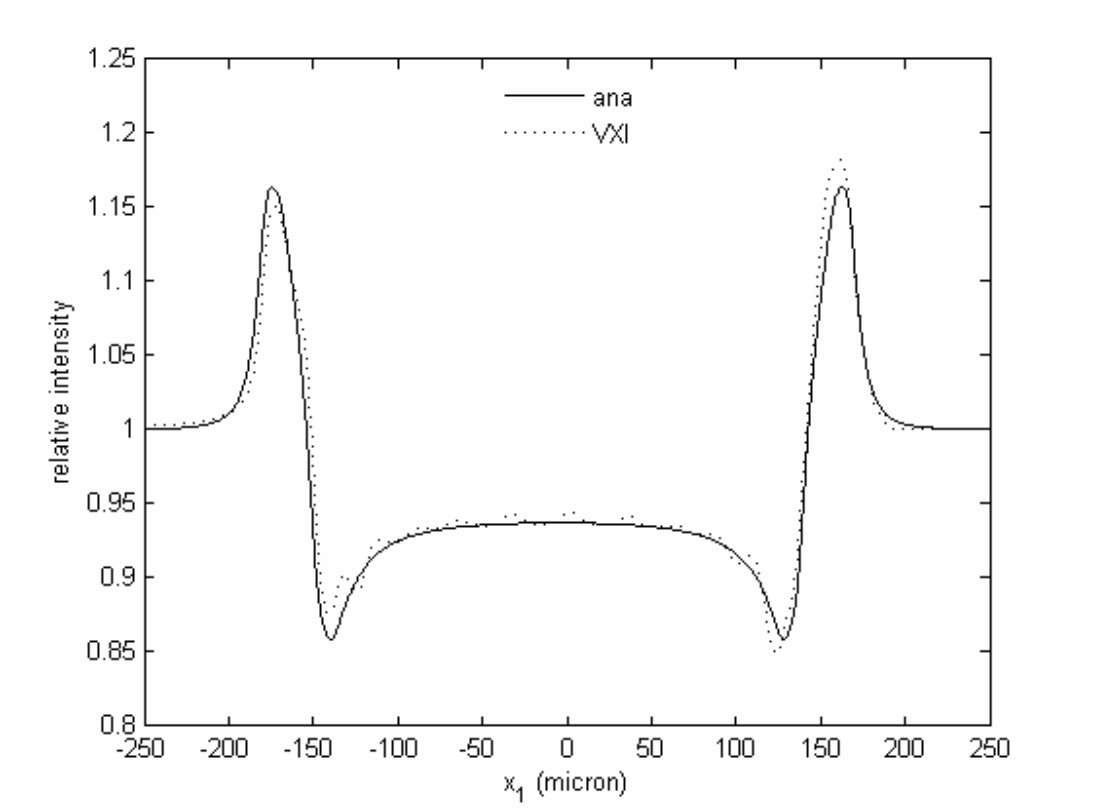
ana
VXI
relative intensity
1.25
1.2
1.15
1.1
1.05
1
0.95
0.9
0.85
0.8
-250
-200
-150
-100
-50
0
50
100
150
200
250
x1 (micron)

Fig. 4e

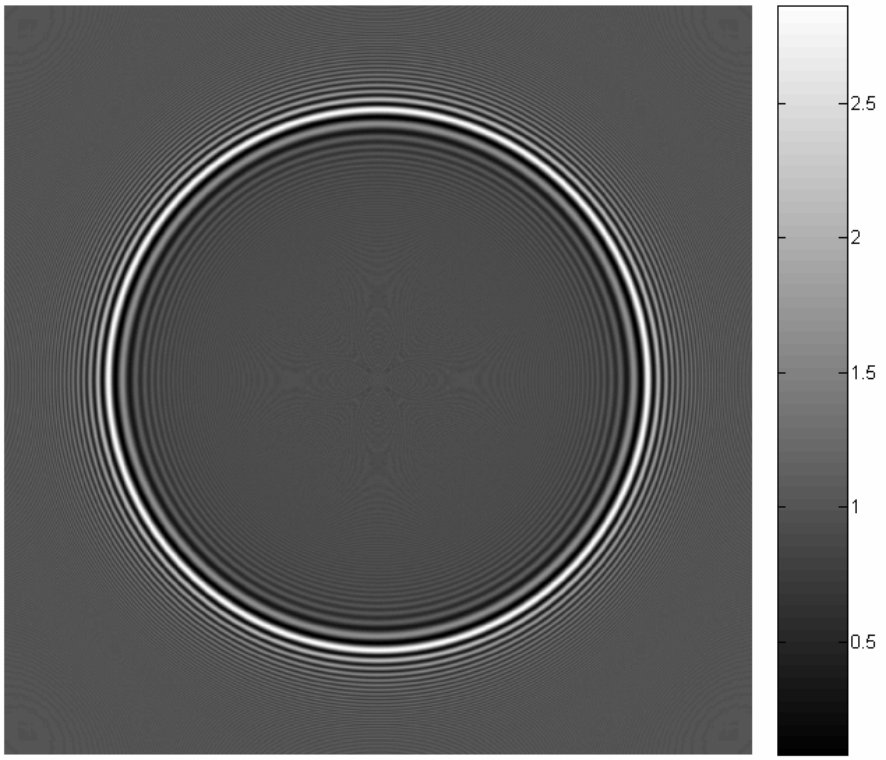

Fig. 4f

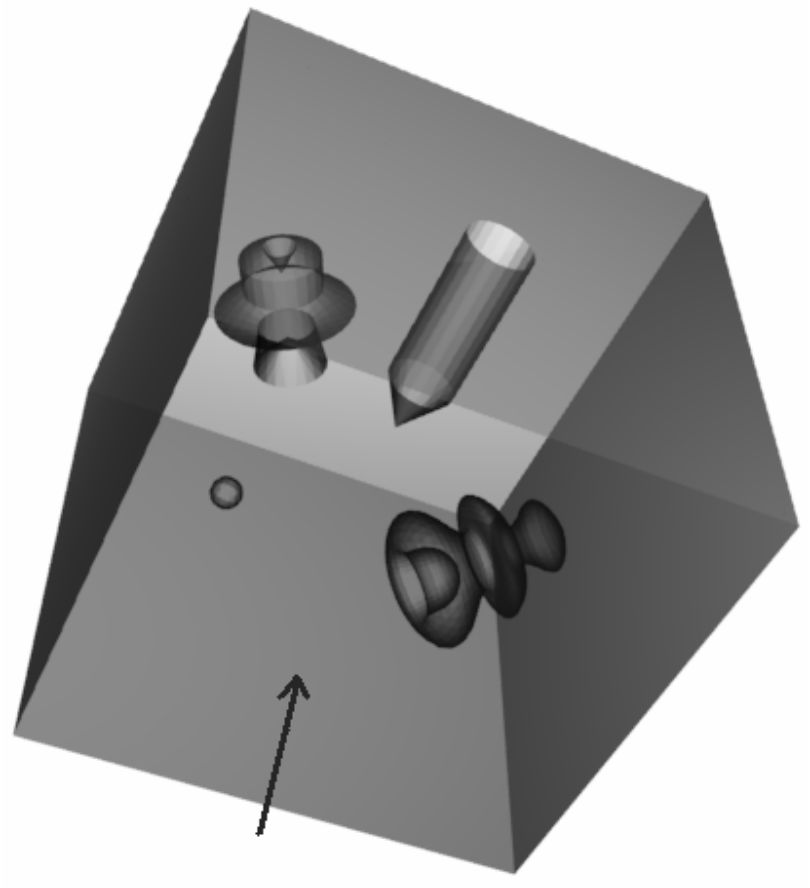

Fig. 5

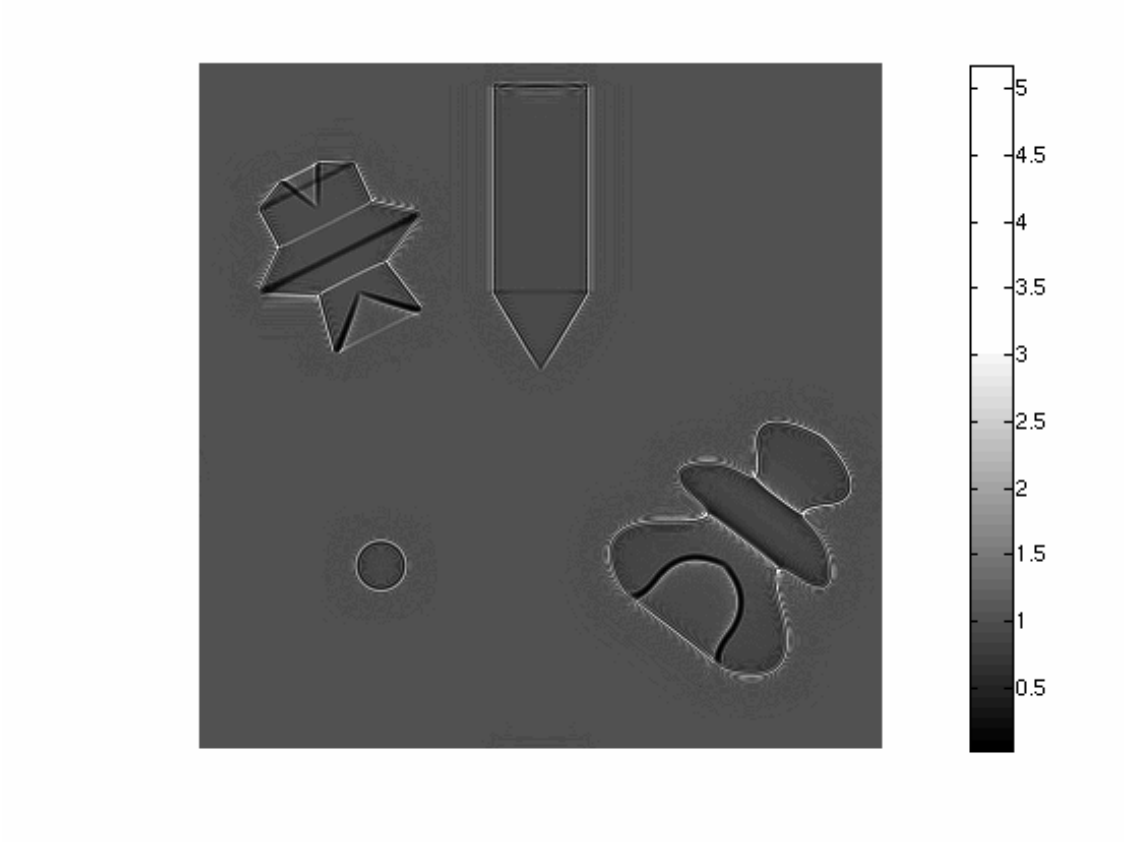

Fig. 6a

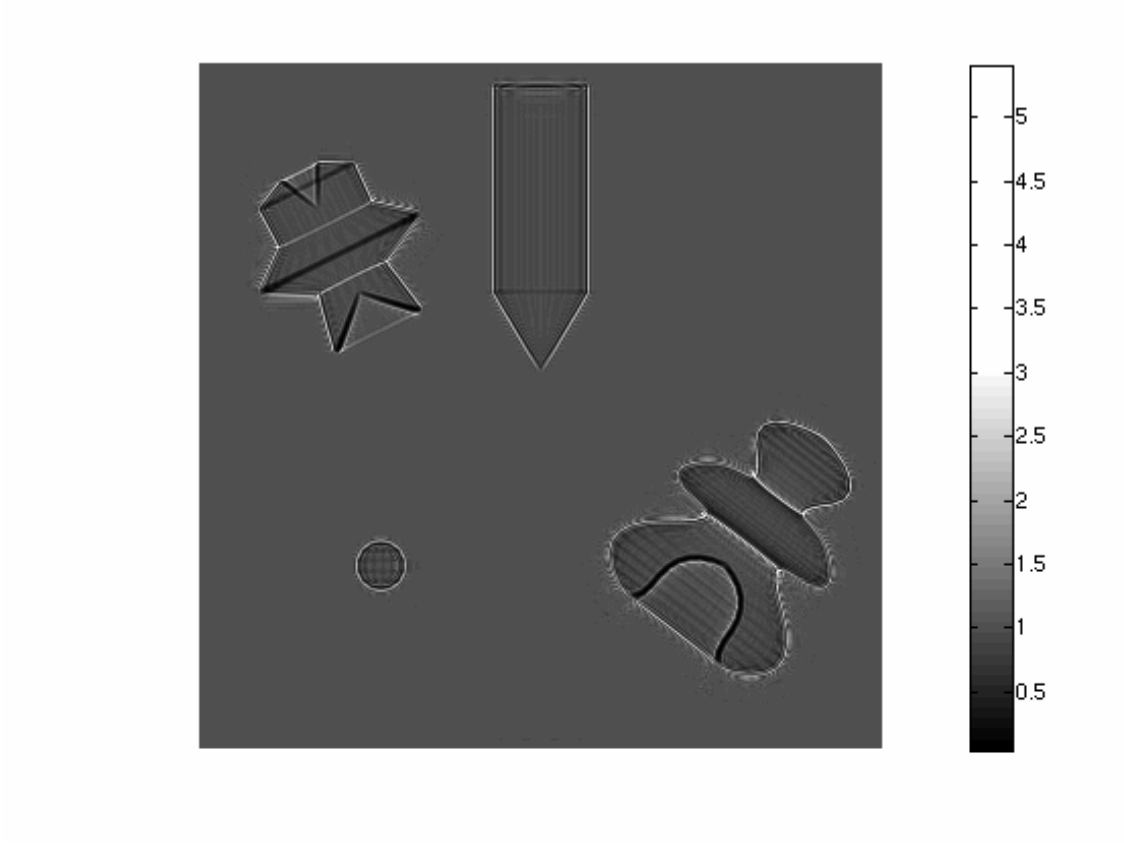

Fig. 6b

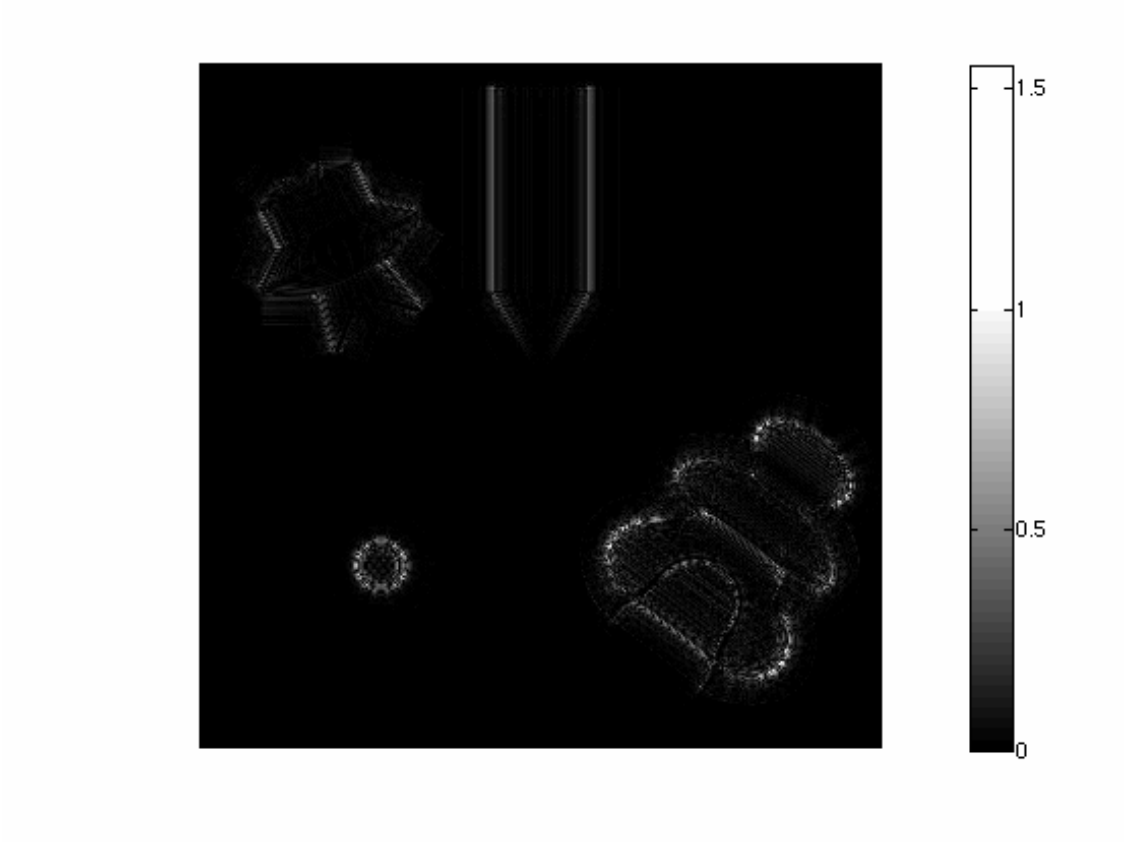

Fig. 6c

Fig. 6d

Fig. 6e

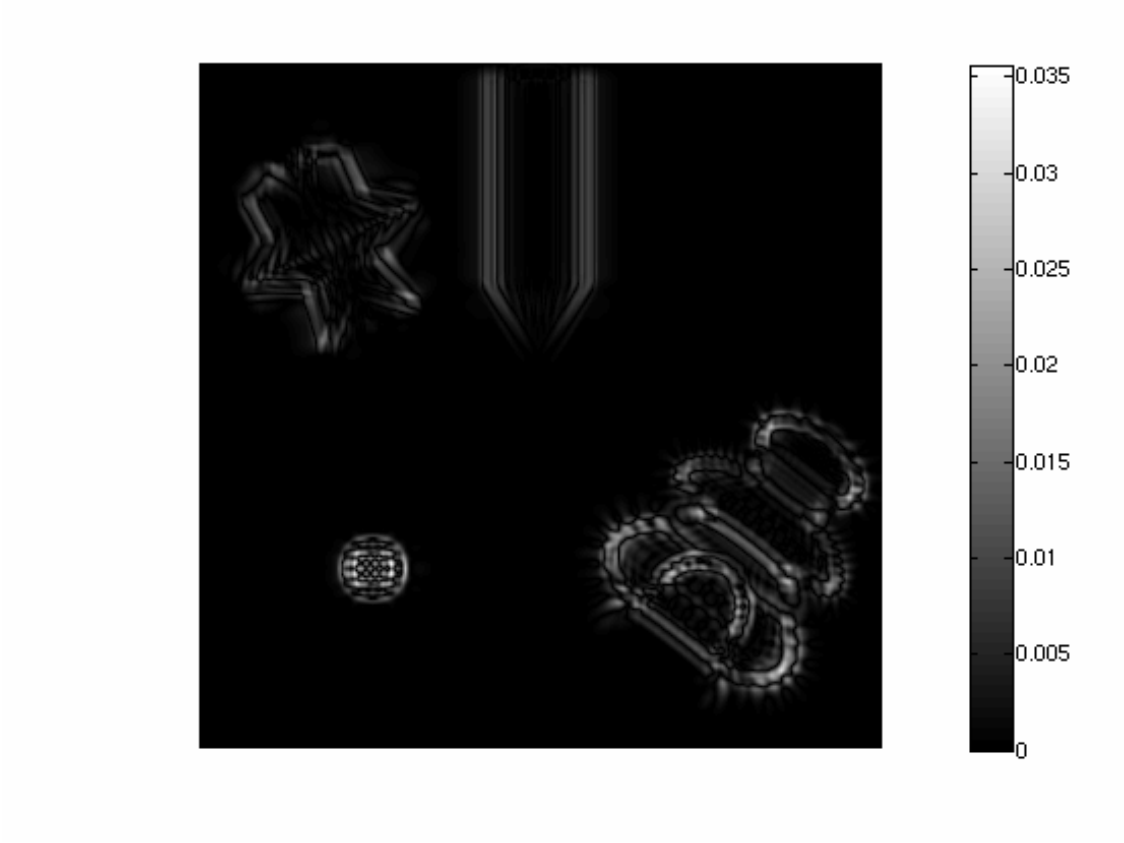

Fig. 6f